

Effect of Sleeve Plunge Depth on Microstructure and Mechanical Properties of Refill Friction Stir Spot Welding of 2198 Aluminum Alloy

Yumei Yue, Yao Shi, Shude Ji, Yue Wang, and Zhengwei Li

(Submitted January 17, 2017; in revised form May 17, 2017; published online September 20, 2017)

Refill friction stir spot welding (RFSSW) is a new spot welding technology, by which spot joint without keyhole can be obtained. In this work, RFSSW was used to join 2-mm-thick 2198-T8 aluminum alloy sheets and effects of the sleeve plunge depth on microstructure and lap shear properties of the joints were mainly discussed. Results showed that when using small plunge depths of 2.4 and 2.6 mm, joints showed good formation and no defects were observed. Incomplete refilling defect was observed with increasing plunge depth due to material loss during welding. Size of the grains at sleeve-affected zone (SAZ) is smaller than that at the pin-affected zone, and the size becomes bigger with increasing the plunge depth. More secondary phase particles can be observed at SAZ with increasing the sleeve plunge depth. The lap shear failure load firstly increased and then decreased with increasing the sleeve plunge depth. The maximum failure load of 9819 N was attained with plug fracture mode when using 2.6 mm. Fracture morphologies show ductile fracture mode.

Keywords defects, lap shear failure load, microstructure, refilling friction stir spot welding, sleeve plunge depth

1. Introduction

Refill friction stir spot welding (RFSSW) is a new variant of friction stir spot welding (FSSW) process (Ref 1). The most outstanding advantage of RFSSW process is that it can join materials without leaving keyholes, which always appear at traditional FSSW joint center and can induce serious stress concentration when FSSW joint bears external forces (Ref 2). Similar to traditional FSSW joint, RFSSW joints also own advantages of smaller distortion, less defect, longer fatigue lives and lower costs since the RFSSW is also a solid-state welding method (Ref 3). Since its invention, the RFSSW process is considered as a promising way to replace traditional spot joining technologies such as riveting and resistance spot welding method (Ref 4, 5).

During traditional FSSW process, the plastic material which is squeezed out by the rotating tool stays at the joint edge, forming flash. After tool retreating, no extra procedures are adopted. The flash cannot be refilled into joint, and therefore, a keyhole is left in joint center at the end of welding process (Ref 6). However, during RFSSW process, the tool system is more complicated than that of the traditional FSSW process. It consists of a pin, a sleeve and a clamping ring. The three components were controlled by three independent actuators

(Ref 7). By simultaneously exerting different movements to the three components, the plastic material which is squeezed out can be refilled into joint after welding (Ref 8-10). Spot joints without keyhole can be obtained in the end. Based on which part of the tool plunging and mainly stirring the material, the RFSSW process can be clarified into sleeve plunge type and pin plunge type. The sleeve plunge RFSSW can fabricate joints with larger bonding area and therefore attracts more attention. The schematic illustration of the sleeve plunge RFSSW has been widely introduced in references and is shown in Fig. 1 (Ref 11). The RFSSW process can be divided into four stages: friction-heating stage, plunging stage, refilling stage and joint-forming stage. During RFSSW, pin and sleeve can independently rotate and move. At friction-heating stage, the clamping ring fixes plates to be welded tightly against the backing board. Both sleeve and pin rotate to produce frictional heat to soften the plates. Then the sleeve plunges downwards and the pin moves upwards, forming a reservoir to accommodate the plastic material. After the sleeve achieved a predetermined depth, the sleeve retracts and the pin moves to the original surface of the plate. During this stage, the displaced plastic material is refilled back into the joint. Joint without keyhole is therefore attained.

Since the invention of RFSSW process, some works have been done to investigate the microstructure and mechanical properties of RFSSW joints (Ref 12-27). Li et al. (Ref 12) studied the microstructure and mechanical properties of 2024-T4 aluminum alloy RFSSW joint and found out that shear-plug fracture mode and shear fracture mode can be obtained during lap shear tests. Gao et al. (Ref 15) found that for 2A97 aluminum alloy, the RFSSW joint after solution and aging treatment owned better mechanical properties than the base material (BM). Tier et al. (Ref 17) reported that reducing the rotational speed from 1900 to 900 rpm increased the bonding ligament length and lap shear failure load of the 5042 RFSSW joint. Cao et al. (Ref 19) reported that an increase in rotational speed, joining time or plunge depth increased the hook height and resulted in lower joint strength. Besides, Shen et al. (Ref

Yumei Yue, Yao Shi, Shude Ji, and Yue Wang, Faculty of Aerospace Engineering, Shenyang Aerospace University, Shenyang 110136, People's Republic of China; and Zhengwei Li, State Key Laboratory of Advanced Welding and Joining, Harbin Institute of Technology, Harbin 150001, China. Contact e-mails: superjds@163.com and qingdaolzw@163.com.

21) reported that the bonding strengths of the thermo-mechanically affected zone/stir zone (TMAZ/SZ) interface and the bonding ligament were the two main regions affecting joint mechanical properties.

According to the Ref 9, 17, and 19, it can be concluded that the tool plunge depth is one of the most significant factors affecting the microstructure and mechanical properties of RFSSW joints. According to Li et al. (Ref 25), different tool plunge depth can change hook morphologies, resulting in different effective sheet thickness and therefore different fracture modes. Zhao et al. (Ref 26) reported that different plunge depths changed the bonding ligament position and further changed the fracture modes. 2198 aluminum alloy is a kind of high-strength aluminum alloy, which owns low density,

high specific modulus, specific strength and good anti-corrosion properties. 2198 alloy is considered as one of the most ideal structure materials for aerospace and aircraft vehicles (Ref

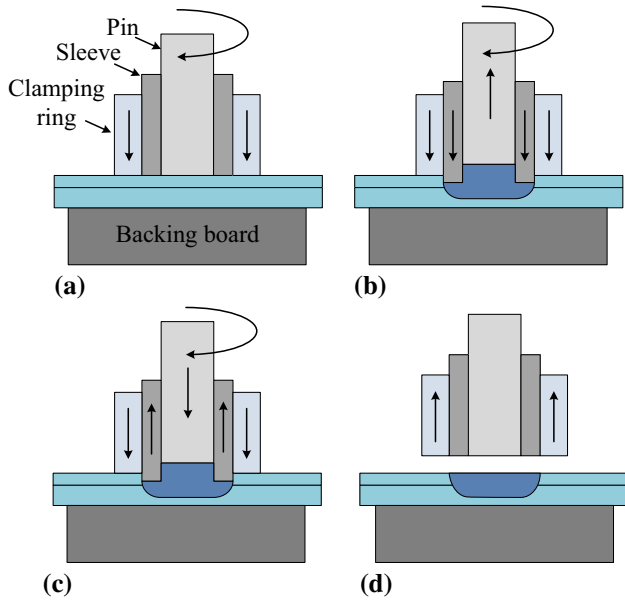


Fig. 1 Schematic illustration of RFSSW processes: (a) stage one, (b) stage two, (c) stage three and (d) stage four

Table 1 Chemical composition of 2198 alloy (wt.%)

Element	Li	Cu	Mg	Mn	Zn	Zr	Ag	Si	Fe	Al
Wt.%	0.98	3.29	0.36	0.05	0.35	0.16	0.30	0.12	0.15	Bal.

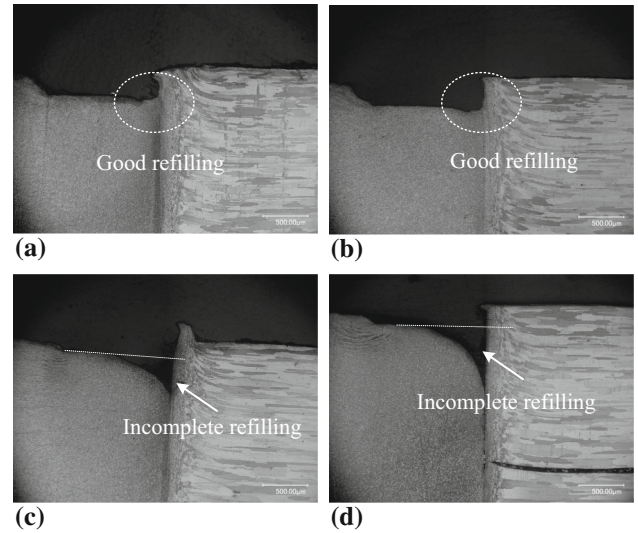


Fig. 3 TMAZ/SZ interface near the joint upper surface: (a) 2.4 mm, (b) 2.6 mm, (c) 2.8 mm and (d) 3.0 mm

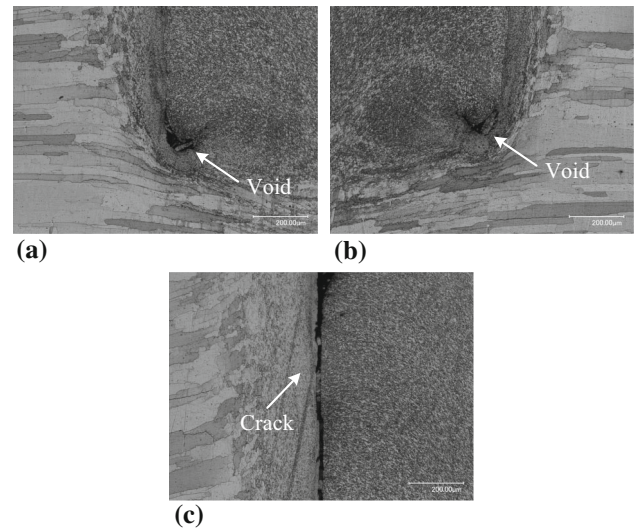


Fig. 4 Defects of the joints when using plunge depth of 3.0 mm: (a) and (b) voids, (c) crack

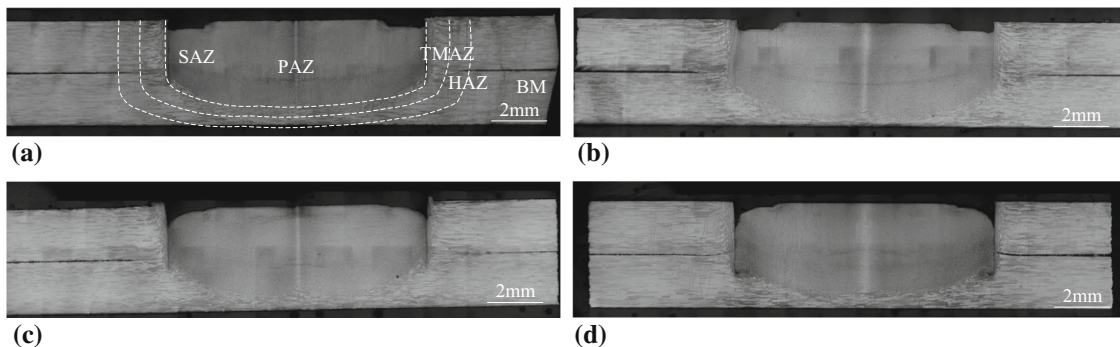


Fig. 2 Cross sections of the RFSSW joints using different plunge depths: (a) 2.4 mm, (b) 2.6 mm, (c) 2.8 mm and (d) 3.0 mm

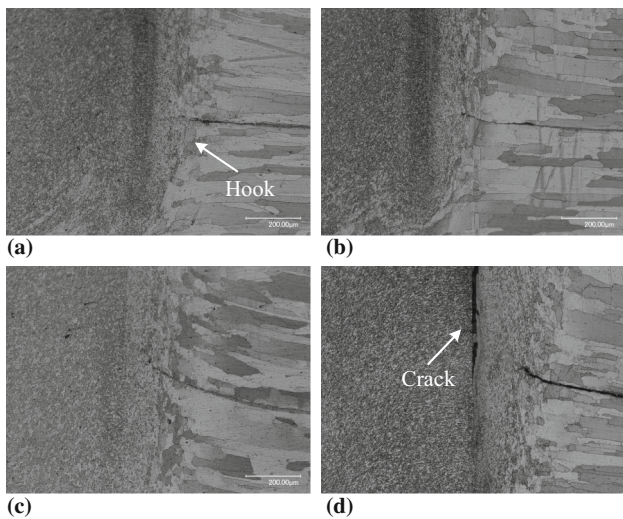


Fig. 5 Hook morphology of the RFSSW joints using different plunge depths: (a) 2.4 mm, (b) 2.6 mm, (c) 2.8 mm and (d) 3.0 mm

27). This focus of this work mainly concentrate on effect of the sleeve plunge depth on microstructure and mechanical properties of the 2198 aluminum alloy RFSSW joints.

2. Experiment

Sheets of 2-mm-thick 2198-T8 aluminum alloy were used to produce the RFSSW joints in this work. The chemical composition is shown in Table 1. Before welding, all sheets were machined to dimensions of 150 mm × 40 mm. The sheets were then cleaned with emery papers to wipe off the oxidations. Two sheets were overlapped and were joined in the center of the overlapped area. The welding processes were performed using an RFSSW machine named RPS100 SK10. The tool used during the experiment consisted of a 18-mm-diameter clamping ring, a 9-mm-diameter sleeve and a 5.2-mm-diameter pin. The tool was made of H13 steel. The outer walls of both the pin and the sleeve were threaded to enhance the material flow behavior during welding. In fact, there exist two variant of RFSSW processes: the pin plunge variant and the sleeve plunge variant. During the pin plunge variant, it is the pin that mainly stirs the material. Similarly, during the sleeve plunge variant, the sleeve mainly stirs the material. In this work, the sleeve plunge variant was used to weld 2198 Al. However, the pin still owns threads on its outer wall. The thread width and depth are 0.8 and 0.3 mm, respectively. The thread pitch is 2 mm. Each of the three components is controlled by an independent actuator system and can be moved up and down independently. And all the three components adopted clearance fit to avoid direct friction from each other. Four different plunge depths 2.4, 2.6, 2.8 and 3.0 mm were used during welding. Other welding parameters such as tool rotating speed, dwell time after plunge, tool plunging speed and retracting speed were 1600 rpm, 0.5 s, 60 and 60 mm/min, and the welding parameters were kept constant during the whole experiment. After welding, the metallographic samples were cut using an electrical discharge cutting machine. Metallographic samples were etched with Keller's reagent for 20 s. Then the metallographic analyses were carried out by optical microscopy (OM VHX-1000E) and

a scanning electron microscope (SEM FEI Quanta 200F). Lap shear tests were carried out using a computer-controlled universal tensile testing machine using a constant speed of 5 mm/min at room temperature. Shims of the same material and thickness as the specimens were used when clamping the samples during lap shear tests (Ref 17). After the lap shear test, the fracture positions were studied with OM and fracture morphologies were studied using a SEM (SU3500).

3. Results and Discussion

The cross sections of the RFSSW joints using different sleeve plunge depths are shown in Fig. 2. It is seen that keyholes can be successfully refilled after RFSSW process. On the whole, the SZ shows a basin-like morphology, as shown in Fig. 2(a). With increasing the sleeve plunge depth, SZ morphology shows little difference, as shown in Fig. 2(b), (c) and (d). At the joint center, a relative lighter region can be observed. This region is not directly stirred by sleeve and is usually called the pin-affected zone (PAZ). Its grain sizes are obvious different from the other regions of the joint, which will be discussed in the following part.

It is worth mentioning that at the end stage of the welding process, a further plunge of the sleeve is adopted to achieve good bonding of the joint. This is mainly because of the material loss during welding and has been introduced in Ref 26. As shown in Fig. 2(c) and (d), at the TMAZ/SZ interface near joint upper surface, a defect can be observed. Figure 3 shows the magnified view of the TMAZ/SZ interface near joint upper surfaces. It can be seen that when using the plunge depths of 2.4 and 2.6 mm, good material refilling can be observed and no defects can be observed. With increasing the plunge depth to 2.8 and 3.0 mm, an incomplete refilling defect can be observed and size of the defect becomes bigger with increasing the sleeve plunge depth. Shen et al. (Ref 21) attributed the defects to the poor fluidity of the plastic material. In fact, during the RFSSW process, there still exists material loss even though it seems like a process without material loss (Ref 26). Firstly, there exist threads on the outer walls of pin and sleeve. Besides, clearance fits are adopted when assembling the different components of tool as previously introduced. During welding, some plastic material can be extruded into thread grooves and the gaps between different tool components, which will not be refilled into the joint after welding. Hence, the RFSSW process can still results in slight material loss (Ref 26). When using small plunge depth, less heat input is produced, resulting in relative poor material fluidity. Hence, less material will be extruded into the gap, leading to less material loss. With increasing the plunge depth, more frictional heat leads to better material fluidity and more material loss; hence, gradually bigger incomplete refilling can be observed.

As introduced above, big plunge depth leads to a little more serious material loss, which more easily results in defects. Figure 4 shows the defects on the joint using the plunge depth of 3.0 mm. Figure 4(a) and (b) shows that voids can be seen at the maximum plunge depth region. This void can be attributed to insufficient refilling effect induced by material loss. Figure 4(c) shows the crack at the TMAZ/SZ interface. According to Li et al. (Ref 25), weak bonding because of short diffusion time, as well as heat residual stress, can be formed at the TMAZ/SZ interface. The interface can be easily torn once the

residual stress was bigger than the bonding strength. With reducing the distance to joint upper, the bonding gradually become weaker due to gradually decreasing diffusion time. Hence, the crack becomes more serious toward joint upper surface. According to that study, no dimples can be observed at the crack region after the fracture.

For the traditional FSSW joint, the hook always shows an upward bending morphology. This feature can reduce the effective sheet thickness of the upper sheet and is always detrimental to joint mechanical properties. Figure 5 shows the hooks of the RFSSW joints using different plunge depths. It can be seen that when using 2.4 and 2.6 mm, the hook shows a

rather flat morphology and extends toward the joint center, as shown in Fig. 5(a) and (b). This morphology can reduce the effective bonding width of the joint, which is another important factor for lap joints. With increasing the plunge depth, the hook morphology gradually changes from flat to upward, as shown in Fig. 5(c) and (d). Under this condition, the effective sheet thickness of the joint becomes smaller and the effective bonding width becomes bigger accordingly. This hook morphology change can be attributed to the material flow behavior during the RFSSW process. As is well known, plastic material flows downwards along the thread during the welding process. Then it is released at the joint bottom, forming a material

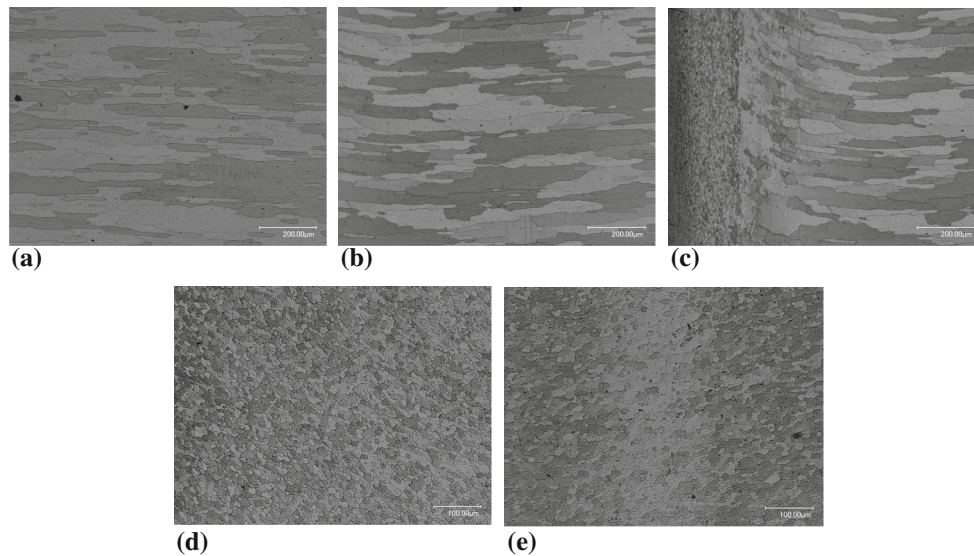


Fig. 6 Microstructures of the RFSSW joints at different regions: (a) BM, (b) HAZ, (c) TMAZ, (d) SAZ and (e) PAZ

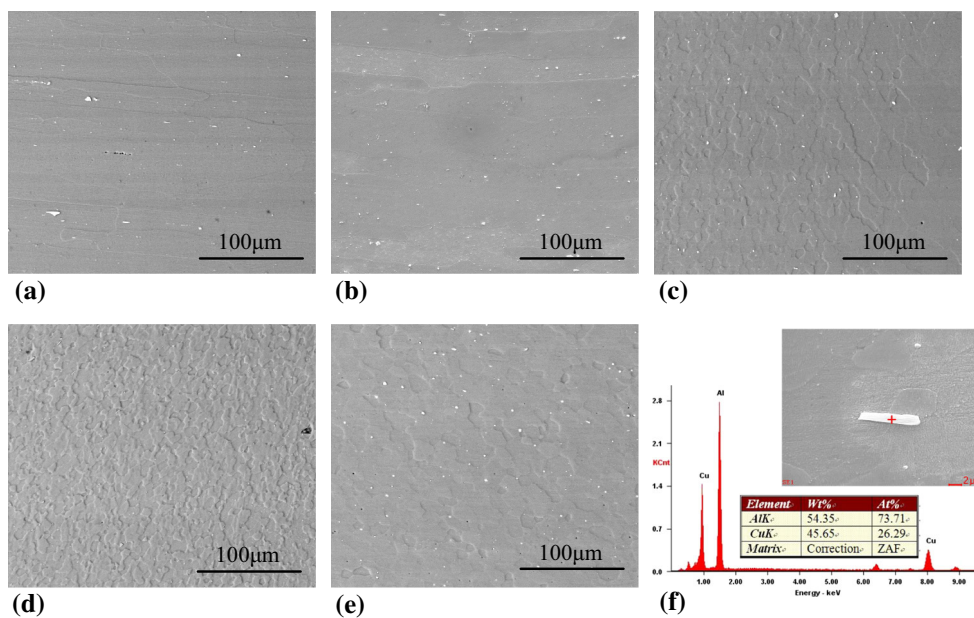


Fig. 7 Distribution of the secondary phase particles at different regions of the joint: (a) BM, (b) HAZ, (c) TMAZ, SZ using 2.4 mm (d) and 3.0 mm (e), (f) the EDS analysis of the secondary particle

accumulated zone. As the welding process goes along, more plastic will be released at the joint bottom; hence, the material accumulated zone becomes bigger, which will force the material relative far away from the joint to bend upwards. So the TMAZ and the hook always present upward morphologies. When using small plunge depth, the downward material flow is

weak, resulting in relative flat hook, as shown in Fig. 5(a) and (b). With increasing the plunge depth, stronger downward material flow leads to more serious upward bending hook, as shown in Fig. 5(c) and (d).

As indicated in Fig. 2(a), the microstructure of the RFSSW joint can be divided into four zones, i.e., base material zone (BM), heat-affected zone (HAZ), TMAZ and SZ. Figure 6 shows the microstructure at different regions of the joint. As shown in Fig. 6(a), in the BM, the grains are elongated along the rolling direction with irregular boundaries. Only undergone the heat cycle during welding and no mechanical stirring action, the microstructure in the HAZ present similar but a little coarser grain structures compared with the BM, as shown in Fig. 6(b). As shown in Fig. 6(c), strongly distorted grains can be observed at the TMAZ due to both the heat cycle and the stirring action of the tool. In the TMAZ region, it can be seen that at the region near the SZ, inhomogeneous grains can be observed, indicating partial dynamic recrystallization process. As shown in Fig. 6(d), the SZ material undergoes intense mechanical stirring during welding and complete dynamic recrystallization happens. Therefore, fine and equiaxed grains can be observed. The average grain size in the PAZ is about $12 \pm 3 \mu\text{m}$. As introduced in Fig. 2, the PAZ owns different microstructures compared with the SZ. Figure 6(e) shows the microstructure of the PAZ. It is obvious that coarser grains ($15 \pm 3 \mu\text{m}$) are obtained due to weak material flow behavior.

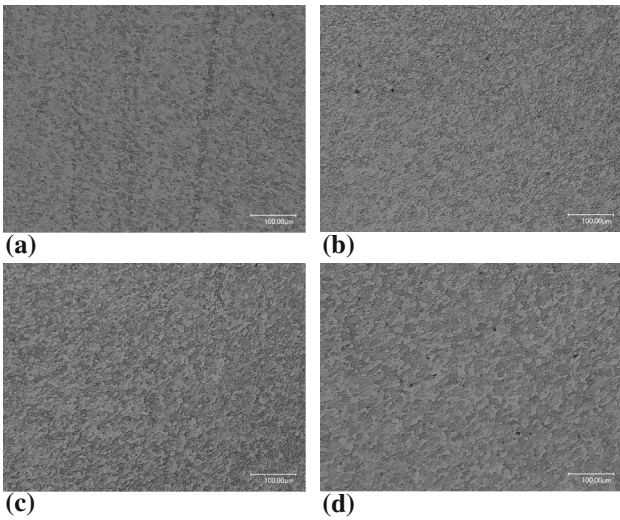


Fig. 8 SAZ of RFSSW joints using different plunge depths: (a) 2.4 mm, (b) 2.6 mm, (c) 2.8 mm and (d) 3.0 mm

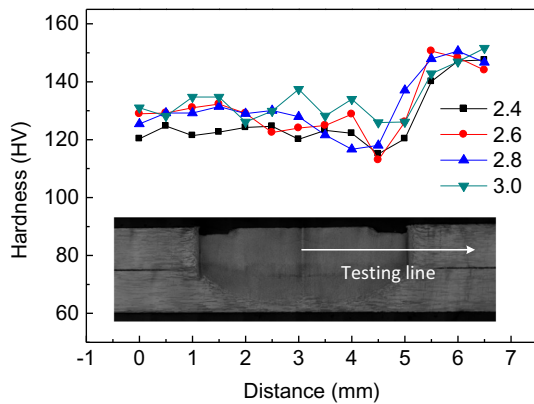


Fig. 9 Hardness of the RFSSW joints

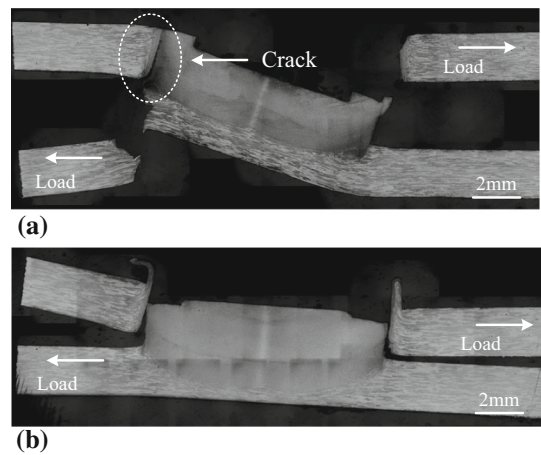


Fig. 11 Fracture modes of the RFSSW joints: (a) plug fracture and (b) shear-plug fracture mode

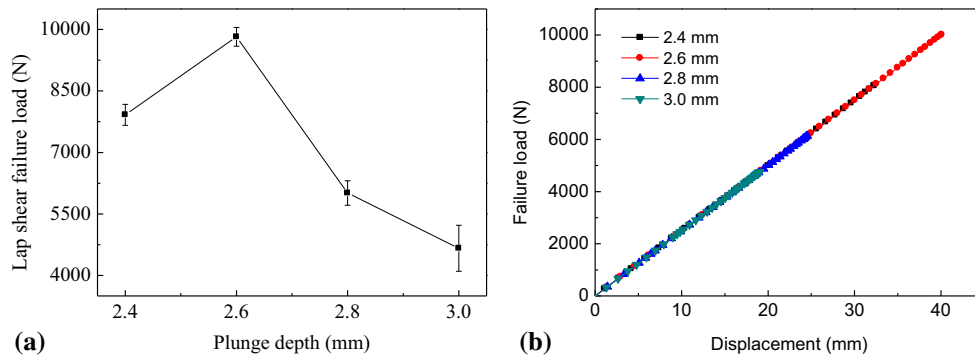


Fig. 10 Lap shear failure loads (a) and load–displacement curves (b) of the RFSSW joint using different plunge depths

2198-T8 aluminum alloy is a precipitation strengthened aluminum alloy. As shown in Fig. 6, the secondary phase particles present black spots among the grains. Figure 7 shows the secondary phase particles at different regions of the joint. The phases distribute both in the grains and at the grain boundaries in the BM region, as shown in Fig. 7(a). As shown in Fig. 7(b), the secondary phase particles show similar distribution and sizes in the HAZ. At the TMAZ, it can be seen that quantity of the phases are much less than that at the BM and the HAZ, as shown in Fig. 7(c). In the SZ, the particles broke into fine particles and distributed homogenously. It can also be seen that the phases in the SZ are much smaller than other regions of the joint, which can be attributed the heat cycle during welding, as shown in Fig. 7(d). Figure 7(e) shows the secondary phase particles using 3.0 mm. It can be seen that more phases than the SZ using 2.4 mm can be observed. Figure 7(f) shows the EDS analysis of the secondary phase particles. The element ratio shows that the phase is possibly the Al_2Cu phase.

As introduced in Fig. 6, the SZ material undergoes complete dynamic recrystallization, and therefore, fine and equiaxed grains can be observed. As is well known, grain sizes of the SZ in FSSW joint can be influenced by the heat input during welding. Traditionally, more heat input always results in bigger grain size, which agrees with the phenomenon of this work. Figure 8 shows the microstructure of the SZ using different plunge depth. It can be seen that sizes of the grains gradually become bigger (from 8 ± 3 to 10 ± 3 , 12 ± 3 and 15 ± 3 μm) with increasing the plunge depth. This can be attributed to more frictional heat caused by big sleeve plunge depth.

Figure 9 shows the hardness values of the RFSSW joints using different sleeve plunge depths. The testing region is the center line of the upper sheet, as shown in Fig. 9. The HXD-1000 machine was used. The testing distance was 0.5 mm and the load was 200 g. It can be seen that from the joint center to the BM, the hardness value firstly decreases and then increases. The hardness shows similar values at SAZ and PAZ and presents an obvious decrease at the TMAZ/SZ interface. Besides, Figure 9 shows that the hardness value gradually increases with increasing the plunge depth. 2198 Al is a kind of precipitation strengthening aluminum alloy. Its hardness values

are affected both by the grain sizes and by the secondary phase particles. Although the grain size using big plunge depth is bigger than that using small plunge depth (Fig. 8), more secondary phase particles are shown in Fig. 7(e) using 3.0 mm. Therefore, it is concluded that the higher hardness using 3.0 mm is mainly determined by the secondary phase particles.

Figure 10(a) shows the lap shear failure load of the joints using different plunge depths. It can be seen that with increasing the plunge depth, the lap shear failure load of joint firstly increases and then decreases. The maximum failure load of 9819 N is attained when using 2.6 mm. The minimum failure load of 4662 N is attained when using 3.0 mm. The load–displacement curves of the joints are shown in Fig. 10(b). It can be seen that all the curves show rather straight morphologies with increasing the displacements. In general, the joints having bigger failure load own bigger displacements. Figure 11 shows the fracture modes of joints. Two fracture modes, the plug fracture mode and the shear-plug fracture mode, can be obtained. Therein, plug fracture modes can be obtained when the plunge depths are 2.4 and 2.6 mm. Shear-plug fracture mode can be obtained when the plunge depth are 2.8 and 3.0 mm. Showing the same fracture mode in Fig. 10(a), the lap shear properties of joints using 2.4 and 2.6 mm were mainly determined by the bonding strength of the TMAZ/SZ interface at upper sheet. As introduced in the study of Li et al. (Ref 25), the bonding strength of TMAZ/SZ interface is mainly affected by heat input. The heat input using the plunge depth of 2.6 mm is higher than that using 2.4 mm. Hence, lap shear failure load increases from 2.4 to 2.6 mm. However, as shown in Fig. 3, incomplete refilling can be obtained when using 2.8 and 3.0 mm due to the material loss during welding. And a serious crack defect can be observed when using 3.0 mm. The bonding strength at the TMAZ/SZ interface is rather weak under this condition. Furthermore, Fig. 5 shows that the hook gradually changes from flat to upward bending morphology with increasing the sleeve plunge depth, further reducing the effective sheet thickness. Therefore, when using big plunge depth, shear-plug fracture mode and lower lap shear failure load can be obtained. It is worth mentioning that in the study of Li et al. (Ref 25), they reported that the maximum lap shear failure load was obtained when the shear-plug fracture mode was

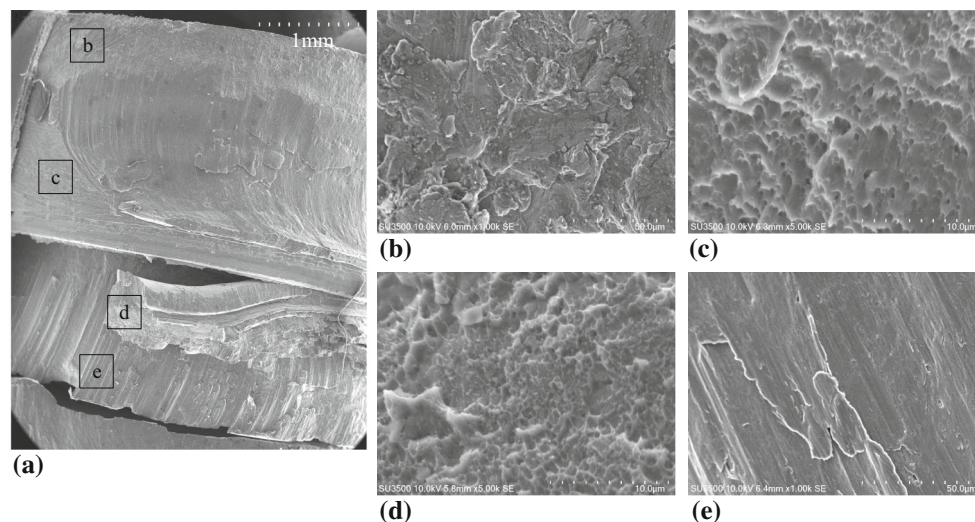


Fig. 12 Fracture morphologies of the plug fracture mode

obtained and plug fracture mode was obtained when using big plunge depth. The difference between the two works can be attributed to the BM material and the different sheets thicknesses. In that paper, the base material was Alclad 2024-T4 Al. The surfaces of BM were covered with Alclad layers to protect its inner alloys. Alclad layer was composed of pure Al, which had much lower strength compared with the 2024 Al. When the joints bear external forces, Alclad layer was prone to crack propagation. Besides, defects such as crack and incomplete refilling easily appear at TMAZ/SZ interface. Therefore, the joint strength in that paper was mainly determined by the strengths of Alclad layer in joint center and the TMAZ/SZ interface. Moreover, in that study, the thicknesses of lower sheets were bigger than that of the upper sheet. Shear-plug fracture mode was easily attained under that condition.

Figure 12 shows the fracture morphologies of the plug fracture mode. Figure 12(a) shows the general view of the fracture surface, in which the upper and the lower sheets can be clearly recognized. Figure 12(b), (c), (d) and (e) shows the fracture morphologies of different regions. Figure 12(b) shows the TMAZ/SZ interface near the joint upper surface. According to Li et al. (Ref 25), very weak bonding is formed at this region and torn is easily formed. Therefore, no obvious dimples can be observed at this region. Figure 12(c) shows the lower region of the TMAZ/SZ interface on the upper sheet. Longer diffusion time leads to better bonding at this region, and therefore, dimples with different sizes can be observed, indicating ductile fracture mode. Figure 12(d) shows the fracture morphology at the lower sheet. This region is the main deformation region during the lap shear tests. Hence, a plenty of dimples can be observed. Figure 12(e) shows the final fracture region. It fractures during a very short time; therefore, only some ridge-like structures can be observed.

4. Conclusions

In this work, 2-mm-thick 2198-T8 aluminum alloy was welded using RFSSW. The effect of the sleeve plunge depth on microstructure and mechanical properties of the joints was mainly discussed. The following conclusions can be drawn.

- (1) When using plunge depths from 2.4 to 2.6 mm, RFSSW joint with good formation can be obtained. With increasing the plunge depth to 2.8 mm, an incomplete refilling defect can be observed due to the material loss during welding.
- (2) Grains and secondary phase particles show rather different distribution and size at different regions of the joint. With increasing the sleeve plunge depth, grain with bigger sizes and more secondary phase particles can be observed in the SZ.
- (3) Lap shear failure load of the joint firstly increases and then decreases with increasing the sleeve plunge depth. The maximum failure load of 9819 N is attained when using 2.6 mm.
- (4) Plug fracture mode with high lap shear failure load is attained when using small plunge depth. Shear-plug fracture mode is obtained due to the incomplete refilling and the upward bending hook when using big plunge depth.

Acknowledgments

This work is supported by the National Natural Science Foundation of China (Nos. 51204111 and 51405309), the Program for Liaoning Excellent Talents in University (No. LJQ2015084) and the Aeronautical Science Foundation of China (2014ZE54021).

References

1. Y.Q. Zhao, H.J. Liu, Z. Lin, S.X. Chen, and J.C. Hou, Microstructures and Mechanical Properties of Friction Spot Welded Alclad 7B04-T74 Aluminium Alloy, *Sci. Technol. Weld. Join.*, 2014, **19**(7), p 617–622
2. Z. Shen, X. Yang, S. Yang, Z.H. Zhang, and Y.H. Yin, Microstructure and Mechanical Properties of Friction Spot Welded 6061-T4 Aluminum Alloy, *Mater. Des.*, 2014, **54**, p 766–778
3. Z. Li, Y. Yue, S. Ji, C. Peng, and L. Wang, Optimal Design of Thread Geometry and Its Performance in Friction Stir Spot Welding, *Mater. Des.*, 2016, **94**, p 368–376
4. S. Venukumar, S. Muthukumar, S.G. Yalagi, and S.V. Kailas, Failure Modes and Fatigue Behavior of Conventional and Refilled Friction Stir Spot Welds in AA6061-T6 Sheets, *Int. J. Fatigue*, 2014, **61**, p 93–100
5. Y. Uematsu, K. Tokaji, Y. Tozaki, T. Kurita, and S. Murata, Effect of Re-filling Probe Hole on Tensile Failure and Fatigue Behavior of Friction Stir Spot Welded Joints in Al–Mg–Si Alloy, *Int. J. Fatigue*, 2008, **30**, p 1956–1966
6. T. Pan, M. Santella, and N. Blundell, Friction Stir Spot Welding for Structural Aluminum Sheets, *SAE Int. J. Mater. Manuf.*, 2009, **2**(1), p 23–29
7. Z. Shen, Y. Chen, J.S.C. Hou, X. Yang, and A.P. Gerlich, Influence of Processing Parameters on Microstructure and Mechanical Performance of Refill Friction Stir Spot Welded 7075-T6 Aluminum Alloy, *Sci. Technol. Weld. Join.*, 2015, **20**(1), p 48–57
8. J.A.E. Mazzaferro, T.S. Rosendo, C.C.P. Mazzaferro, F.D. Ramos, M.A.D. Tier, T.R. Strohaecker, and J.F. dos Santos, Preliminary Study on the Mechanical Behavior of Friction Spot Welds, *Soldagem Insp.*, 2009, **14**(3), p 238–247
9. G. Pieta, J. dos Santos, T.R. Strohaecker, and T. Clarke, Optimization of Friction Spot Welding Process Parameters for AA2198-T8 Sheets, *Mater. Manuf. Process.*, 2014, **29**(8), p 934–940. doi: [10.1080/10426914.2013.811727](https://doi.org/10.1080/10426914.2013.811727)
10. M.A.D. Tier, J.F. dos Santos, T. Rosendo, J.A.E. Mazzaferro, and A.A.M. Silva, The Influence of Weld Microstructure on Mechanical Properties of Alclad AA2024-T3 Friction Spot Welded. in *SAE Technical Paper*: 2008-01-2287
11. A. Patnaik, K. Koch, W. Arbegast, and C. Allen, Static properties of “refill” friction spot welded skin stiffened compression panels. in *SAE Technical Paper*: 2006-01-0967
12. Z. Li, S. Gao, S. Ji, Y. Yue, and P. Chai, Effect of Rotational Speed on Microstructure and Mechanical Properties of Refill Friction Stir Spot Welded 2024 Al alloy, *J. Mater. Eng. Perform.*, 2016, **25**(4), p 1673–1682
13. U.F.H. Suhuddin, V. Fischer, and J.F. dos Santos, The Thermal Cycle During the Dissimilar Friction Spot Welding of Aluminum and Magnesium Alloy, *Scripta Mater.*, 2013, **68**, p 87–90
14. A.H. Plaine, U.F.H. Suhuddin, N.G. Alcântara, and J.F. dos Santos, Fatigue Behavior of Friction Spot Welds in Lap Shear Specimens of AA5754 and Ti6Al4 V Alloys, *Int. J. Fatigue*, 2016, **91**, p 149–157
15. C. Gao, R. Gao, and Y. Ma, Microstructure and Mechanical Properties of Friction Spot Welding Aluminium–Lithium 2A97 Alloy, *Mater. Des.*, 2015, **83**, p 719–727
16. C. Gao, Y. Ma, L. Tang, P. Wang, and X. Zhang, Microstructural Evolution and Mechanical Behavior of Friction Spot Welded 2198-T8 Al–Li Alloy During Aging Treatment, *Mater. Des.*, 2017, **115**, p 224–230
17. M.A.D. Tier, T.S. Rosendo, J.F. dos Santos, N. Huber, J.A. Mazzaferro, C.P. Mazzaferro, and T.R. Strohaecker, The Influence of Refill FSSW Parameters on the Microstructure and Shear Strength of 5042 Aluminum Welds, *J. Mater. Process. Technol.*, 2013, **213**, p 997–1005
18. U. Suhuddin, V. Fischer, F. Kroeff, and J.F. dos Santos, Microstructure and Mechanical Properties of Friction Spot Welds of Dissimilar AA5754 Al and AZ31 Mg Alloys, *Mater. Sci. Eng., A*, 2014, **590**, p 384–389
19. J.Y. Cao, M. Wang, L. Konga, and L.J. Guo, Hook Formation and Mechanical Properties of Friction Spot Welding in Alloy 6061-T6, *J. Mater. Process. Technol.*, 2016, **230**, p 254–262

20. A.H. Plaine, U.F.H. Suhuddin, C.R.M. Afonso, N.G. Alcântara, and J.F. dos Santos, Interface Formation and Properties of Friction Spot Welded Joints of AA5754 and Ti6Al4 V Alloys, *Mater. Des.*, 2016, **93**, p 224–231
21. Z. Shen, X. Yang, Z. Zhang, L. Cui, and T. Li, Microstructure and Failure Mechanisms of Refill Friction Stir Spot Welded 7075-T6 Aluminum Alloy Joints, *Mater. Des.*, 2012, **44**, p 476–486
22. A.H. Plaine, A.R. Gonzalez, U.F.H. Suhuddin, J.F. dos Santos, and N.G. Alcântara, The Optimization of Friction Spot Welding Process Parameters in AA6181-T4 and Ti6Al4 V Dissimilar Joints, *Mater. Des.*, 2015, **83**, p 36–41
23. P.H.F. Oliveira, S.T. Amancio-Filho, J.F. dos Santos, and E. Hage, Jr., Preliminary Study on the Feasibility of Friction Spot Welding in PMMA, *Mater. Lett.*, 2010, **64**, p 2098–2101
24. W.S. Junior, T. Emmeler, C. Abetz, U.A. Handge, J.F. dos Santos, S.T. Amancio-Filho, and V. Abetz, Friction Spot Welding of PMMA with PMMA/Silica and PMMA/Silica-g-PMMA Nanocomposites Functionalized via ATRP, *Polymer*, 2014, **55**, p 5146–5159
25. Z. Li, S. Ji, Y. Ma, P. Chai, Y. Yue, and S. Gao, Fracture Mechanism of Refill Friction Stir Spot-Welded 2024-T4 Aluminum Alloy, *Int. J. Adv. Manuf. Technol.*, 2016, **86**(5), p 1925–1932
26. Y.Q. Zhao, H.J. Liu, S.X. Chen, Z. Lin, and J.C. Hou, Effects of Sleeve Plunge Depth on Microstructures and Mechanical Properties of Friction Spot Welded Alclad 7B04-T74 Aluminum Alloy, *Mater. Des.*, 2014, **62**, p 40–46
27. Yu Ma, Z.C. Xia, R.R. Jiang, and W. Li, Effect of Welding Parameters on Mechanical and Fatigue Properties of Friction Stir Welded 2198-T8 Aluminum–Lithium Alloy Joints, *Eng. Fract. Mech.*, 2013, **114**, p 1–11